Pergamon

Int. J. Heat Mass Transfer. Vol. 40, No. 14, pp. 3351–3360, 1997

Printed in Great Britain
0017–9310/97 $17.00+0.00

PII: S0017–9310(96)00368–7

A generalized thermal modeling for laser drilling process—I. Mathematical modeling and numerical methodology

R. K. GANESH and A. FAGHRI†
Mechanical Engineering Department, The University of Connecticut, Storrs, CT 06269-3139, U.S.A.

and

Y. HAHN
Physics Department, The University of Connecticut, Storrs, CT 06269-3046, U.S.A

(*Received* 7 *March* 1996 *and in final form* 29 *October* 1996)

Abstract—Conduction and advection heat transfer in the solid and liquid metal, respectively, the free surface flow of the liquid melt and its expulsion, the tracking of the solid–liquid and liquid–vapor interfaces with different thermo–physical properties in the two phases and the evolution of latent heat of fusion over a temperature range are mathematically modeled for the two-dimensional axisymmetric case in the transient development of a laser drilled hole where the impressed pressure and temperature on the melt surface is provided by a one-dimensional gas dynamics model. Significant improvement made to our earlier melting and solidification submodel is discussed that comprises a temperature transforming model on a fixed grid system. The resulting advection–diffusion equation's compatibility with the present fluid flow simulation model is described. The mathematical formulation of the submodels and the numerical methodology is presented. © 1997 Elsevier Science Ltd.

1. INTRODUCTION

Laser machining has become an accepted manufacturing process nowadays in many industries which include automotive, aerospace, electronic, appliance and material processing [1–3]. However, a trial and error procedure is being followed in the manufacturing process which translates to tremendous amounts of reworking costs and wastage. In order to gain control and increase the efficiency of the process, the modeling of the entire process needs to be undertaken. The laser processes are, it should be borne in mind, very intense, short lived and complex. Many process parameters such as pressure and temperature cannot be routinely measured and to isolate and study the effect of a particular variable is not possible. A computer model based on a numerical model evolved from underlying physical models in conjunction with the insights gained from experimental observations offers a cost effective design tool alternative that will help us gain precise control over many laser manufacturing processes, in particular laser drilling. Towards realizing this objective and help industries, the first and primary step is to build these sound numerical models and this is precisely the reason why the literature is abundant with many numerical models and to a lesser extent with analytical and theoretical ones. Some of these models which are relevant to our present work are listed in Table 1 which presents previous works undertaken by various investigators in the light of different distinct categories, namely the dimensionality of the problem, whether or not the energy is taken into account in addition to fluid flow, whether or not the free surface capability exists, whether or not vaporization and solidification (recast formation) are considered in the phase change model, the type of methodology adopted and finally whether or not experimental comparison exists. The last column lists some of the key words associated with their work, for example, drilling velocity and drilling efficiency which were studies by Von Allmen [4] in his model.

As one can see, there is no single model which takes into account all the processes, namely the free surface flow of the melt, multi-phase heat transfer, vaporization gas dynamics and the melting and solidification of the metal substrate, simultaneously in more than one dimension. The task of this paper is to describe one such numerical model with significant improvements made in the melting and solidification submodel.

† Author to whom correspondence should be addressed.

NOMENCLATURE

B	source term in the nonlinear energy equation
c	specific heat [J/kg/K]
c_s	speed of sound [m/s]
C^0	coefficient of the nonlinear term in the temperature function equation (8) [J/kgK]
C^*	dimensionless specific heat
C	ratio of specific heats
$\hat{d}$	direction unit vector
d_0	characteristic length
E	enthalpy [J/kg]
F	volume of fluid function
g	gravitational acceleration, 9.8 [m/s^2]
g^*	dimensionless gravitational acceleration
I	intensity of laser beam [W/m^2]
k	thermal conductivity [W/m/K]
K	ratio of thermal conductivities
K^*	dimensionless thermal conductivity
L	latent heat [J/kg]
$\hat{n}$	unit normal
N	a large number
p	pressure [N/m^2]
p^*	dimensionless pressure
Pr	Prandtl number
r	radial coordinate
r^*	dimensionless radial coordinate
R	specific gas constant [J/kg/K]
S^0	coefficient in equation (8) [J/kg]
S^*	dimensionless coefficient, S^0
Ste	Stefan number
t	time coordinate [s]
t^*	dimensionless time coordinate
T^0	temperature [K]
T^d	temperature difference w.r.t melting temperature [K]
T^*	dimensionless temperature difference
T_m^0	melting or solidification temperature [K]
u, v	velocities [m/s]
u^*, v^*	dimensionless velocities
$\vec{u}$	relative velocity w.r.t. moving phase front
$\vec{v}$	velocity, w.r.t fixed reference frame
z	axial coordinate
z^*	dimensionless axial coordinate.

Greek symbols

α	thermal diffusivity [m^2/s]
δ	semi phase change temperature interval, δT^0 [K]
Δ	change in quantity
γ	ratio of specific heats
μ	dynamic viscosity
ν	kinematic viscosity [m^2/s]
ρ	density [kg/m^3]
σ	surface tension coefficient [N/m]
σ^*	dimensionless surface tension coefficient.

Subscripts

abs	absorbed
c	cold
h	hot
l	liquid phase
lv	fixed reference frame
m	melt
p	pressure
s	solid phase, surface
sl	solid to liquid
v	vapor
vap,0	saturate state.

Superscripts

0	dimensional (temperature)
*	dimensionless (temperature)
d	difference.

In our previous work [5], a direct computer simulation technique was undertaken to understand both qualitatively and quantitatively the influence of fluid flow and heat transfer in the transient development of a laser drilled hole in a turbine airfoil material. The model also treated the laser melted pool surface as a free deformable surface. Melting and solidification [6] were modeled using a switch-on switch-off technique, i.e. when the calculated average cell temperature exceeds that of melting, the cell is switched on to a fluid cell. Solidification (recast formation) was modeled by switching off the fluid cell to a solid one, once the average cell temperature fell below that of melting. The latent heat of fusion was neglected in order to simplify the analysis (it is also a small percentage of the overall heat content of the melt [7]). The purpose of this paper is to present a significantly improved laser drilling model with emphasis on the melting and solidification submodel, relaxing many assumptions that were made in the earlier model. It was assumed in our previous work that the properties k and c_p were the same regardless of the phase. In the improved model there exists the option of specifying the actual properties in the two phases. It was also assumed before that the target material behaved like a pure substance with a single well defined melting temperature. In the improved model, the melting can take place gradually over a temperature range that spans

Table 1. Summary of thermal modeling of laser drilling process

Investigator	Dimension	Fluid Flow	Energy	Free Surface	Phase change		Exp. Methodology	Comparison	Comments
					Vapor	Recast			
Paek and Gagliano [22]	3-D transient	No	Yes	No	No	No	Theoretical	Yes	Temperature profile, tangential stress distribution
Von Allmen [4]	1-D transient	Yes	Yes	No	Yes	No	Analytical	Yes	Drilling velocity, drilling efficiency
Chan and Mazumder [7]	2-D transient	Yes	Yes	No	No	No	Numerical	No	Surface tension driven flow
Kou and Wang [23]	3-D quasi-steady state	Yes	Yes	No	No	No	Numerical	Yes	Surface tension and buoyancy driven flow
Mazumder [24]	3-D quasi-steady state	Yes	Yes	Yes	No	No	Numerical	No	Point by point partially vectorized scheme
Chan and Mazumder [25]	1-D steady state	Yes	Yes	No	Yes	No	Analytical/ Numerical	No	Immobilization transformation, Newton–Raphson method
Basu & Srinivasan [8]	2-D steady state	Yes	Yes	No	Yes	No	Numerical	No	Vorticity-stream function formulation, finite difference method
Zacharia *et al.* [26]	3-D transient	Yes	Yes	Yes	No	No	Numerical	Some	Arc welding, moving arc, DEA method
Kar and Mazumder [27]	2-D transient	No	Yes	No	Yes	No	Analytical/ Numerical	No	Energy, Stefan bc, Runge–Kutta method
Mazumder *et al.* [24]	2-D axisymmetric Q-S state	Yes	Yes	No	No	No	Numerical	No	Effect of convection and Pr on pool geometry
Mazumder *et al.* [24]	2-D axisymmetric, Q-S state	Yes	Yes	No	No	No	Numerical	No	Perturbation, FDM, ADI methods
Mazumder *et al.* [24]	3-D transient	Yes	Yes	No	No	No	Numerical	No	Scanning, FDM, vectorization
Patel & Brewster [28]	2-D steady, axisymmetric	Yes	Yes	No	No	No	Analytical/ Numerical	Yes	Gas assist, 1-D heat conduction, top-hat, Runge-Kutta method
Bellantone, Ganesh *et al.* [5]	2-D transient, axisymmetric	Yes	Yes	Yes	Yes	No	Analytical/ Numerical	Some	Spatial and temporal variations of free surface temperature and pressure
Kar and Mazumder [29]	2-D transient	No	Yes	No	Yes	No	Analytical/ Numerical	No	Gas assist and reflections, Runge–Kutta method
Gordon *et al.* [30]	2-D transient axisymmetric	No	Yes	No	Yes	No	Numerical	No	CVFEM, Landau transformation
Ho *et al.* [31]	1-D transient	No	Yes	No	Yes	No	Numerical	No	2-D axisymmetric gas flow, Crank–Nicholson method
Present	2-D transient axisymmetric	Yes	Yes	Yes	Yes	Yes	Numerical/ Analytical	Some	Generalized thermal model

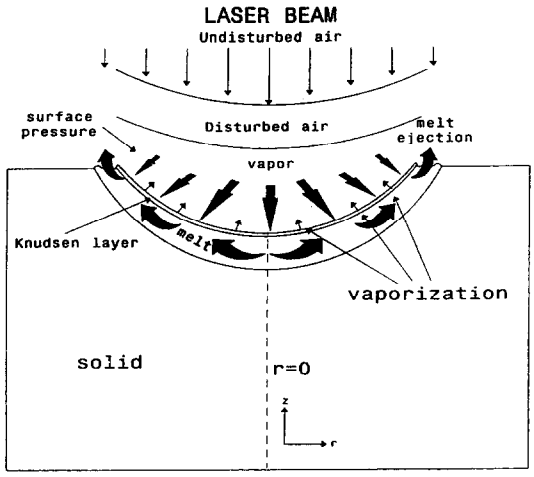

Fig. 1. Schematic diagram of laser drilling process.

the entire mushy zone typically exhibited by alloys and mixtures going through a phase change. Also, the latent heat of fusion is not neglected in the improved model. It was neglected by Chan *et al.* [7] in the interface energy balance based on a low value of latent heat of fusion [8].

A schematic of the laser drilling process is shown in Fig. 1. A laser beam is produced and directed towards a solid target material which absorbs a fraction of the incident light energy. Melting and then vaporization occurs which creates a back pressure on the liquid free surface which in turn pushes the melt away in the radial direction. Thus the material is removed by a combination of vaporization and liquid expulsion. There is a Knudson layer adjacent to the liquid–vapor interface which is only a few microns thick. On top of this layer, lie stacked in the vertical direction, the layers of vapor, disturbed air and undisturbed quiescent air.

The modeling of phase change problems in an engineering situation such as laser drilling can either be a strong numerical (or a classical) solution or a weak fixed grid solution [9, 10]. The former requires either a moving grid or an immobilization coordinate transformation whereas in the latter the solution is obtained on a fixed grid. In a weak temperature based method which starts from the enthalpy form of the energy equation [11], an equivalent specific heat which incorporates the latent heat of fusion is defined as a function of temperature [12, 13]. This method does not impose any constraints on the time step or the grid size [14, 15]. The latent heat release or absorption at the phase front in a system undergoing a phase-change can take plane at a single distinct temperature (for pure substances, isothermal) or over a temperature range (for mixtures or alloys, mushy-region).

2. THEORETICAL DEVELOPMENT

The governing differential equations are the conservation of mass, momentum and energy in two-dimensional (2-D) polar coordinates. The energy equation is to be solved as an advection–diffusion equation that incorporates the phase-change via the temperature based equivalent heat capacity model [12]. This makes the energy equation nonlinear. The temperature field is obtained for a given fixed velocity field for a time step and therefore the energy equation will be discussed after discussing the continuity and momentum equations.

2.1. *Hydrodynamical equations*

The hydrodynamical equations are applicable in the melt region shown in Fig. 1. On the free surface where the laser beam impinges, a normal stress boundary condition is applied and at the solid–liquid interface, no-slip boundary conditions are enforced for the velocity components. The liquid melt is driven radially by the impressed pressure gradient which varies spatially and temporally. The problem is assumed to be 2-D axisymmetric and accordingly the momentum and continuity equations are chosen

$$\frac{\partial u}{\partial r}+\frac{\partial v}{\partial z}+\frac{u}{r}=0 \tag{1}$$

$$\frac{\partial u}{\partial t}+u\frac{\partial u}{\partial r}+v\frac{\partial u}{\partial z}=\frac{\mu}{\rho}\left[\frac{\partial^2 u}{\partial r^2}+\frac{\partial^2 u}{\partial z^2}+\frac{1}{r}\frac{\partial u}{\partial r}-\frac{u}{r^2}\right]-\frac{1}{\rho}\frac{\partial p}{\partial r}$$

$$\frac{\partial v}{\partial t}+u\frac{\partial v}{\partial r}+v\frac{\partial v}{\partial z}=\frac{\mu}{\rho}\left[\frac{\partial^2 v}{\partial r^2}+\frac{\partial^2 v}{\partial z^2}+\frac{1}{r}\frac{\partial v}{\partial r}\right]-\frac{1}{\rho}\frac{\partial p}{\partial z}-g. \tag{2}$$

Equations (1) and (2) are nondimensionalized by introducing the following nondimensionalized variables:

$$u^*=\frac{ud_0}{\alpha_l}\quad v^*=\frac{vd_0}{\alpha_l}\quad g^*=\frac{gd_0^3}{\alpha_l^2}\quad \sigma^*=\frac{\sigma d_0}{\rho\alpha_l^2}$$

$$p^*=\frac{pd_0^2}{\rho\alpha_l^2}\quad r^*=\frac{r}{d_o}$$

$$z^*=\frac{z}{d_o}\quad Pr=\frac{\mu}{\rho\alpha_l}\quad t^*=\frac{t\alpha_l}{d_0^2}. \tag{3}$$

where, g and σ are the acceleration due to gravity and the surface tension coefficient (even though this coefficient does not explicitly appear in the governing differential equations, it has to be prescribed in the input data), respectively. The characteristic length, d_0, is taken as the diameter of a typical laser beam and α_l is the thermal diffusivity of the liquid melt. Pr is the ratio of momentum to thermal diffusivities. Substituting equation (3) into equations (1) and (2) results (dropping of the asterisks) in the following set of nondimensional equations.

$$\frac{\partial u}{\partial r}+\frac{\partial v}{\partial z}+\frac{u}{r}=0 \tag{4}$$

$$\frac{\partial u}{\partial t}+u\frac{\partial u}{\partial r}+v\frac{\partial u}{\partial z}=Pr\left[\frac{\partial^2 u}{\partial r^2}+\frac{\partial^2 u}{\partial z^2}+\frac{1}{r}\frac{\partial u}{\partial r}-\frac{u}{r^2}\right]-\frac{\partial p}{\partial r}$$

$$\frac{\partial y}{\partial t}+u\frac{\partial v}{\partial r}+v\frac{\partial v}{\partial z}=Pr\left[\frac{\partial^2 v}{\partial r^2}+\frac{\partial^2 v}{\partial z^2}+\frac{1}{r}\frac{\partial v}{\partial r}\right]-\frac{\partial p}{\partial z}-g. \tag{5}$$

One of the special features employed in the simulation of the laser drilling process is the treatment of the melt surface as a free deformable surface. Special care is taken to preserve the sharp definition of the free boundaries. A volume of fluid (VOF) function, F, [16] is defined to be unity for a full fluid cell and zero for an empty cell. Standard finite difference approximations are inadequate to handle the volume of fluid function F which is a step function that requires a donor–acceptor flux approximation method to sustain free surfaces. F moves with the fluid and the time dependent motion of F is governed by the equation

$$\frac{\partial F}{\partial t}+u\frac{\partial F}{\partial r}+v\frac{\partial F}{\partial z}=0. \tag{6}$$

2.2. *Energy equation*

The nondimensionalization for the variables r^*, z^*, u^*, v^* and t^* are as defined before and the others are as given below [13]:

$$T^*=\frac{T^0-T_m^0}{T_h^0-T_c^0}\quad C^*=\frac{C^0}{c_l}$$

$$S^*=\frac{S^0}{c_l(T_h^0-T_c^0)}\quad K^*=\frac{k}{k_l}$$

$$\delta T^*=\frac{\delta T^0}{T_h^0-T_c^0}\quad Ste=\frac{c_l(T_h^0-T_c^0)}{L} \tag{7}$$

$$C_{sl}=\frac{c_s}{c_l}\quad K_{sl}=\frac{k_s}{k_l}$$

The nondimensionalized equations become after dropping the superscripts

$$\frac{\partial(CT)}{\partial t}+\frac{\partial(uCT)}{\partial r}+\frac{\partial(vCT)}{\partial z}=\frac{\partial}{\partial r}\left(K\frac{\partial T}{\partial r}\right)+\frac{\partial}{\partial z}\left(K\frac{\partial T}{\partial z}\right)+\frac{1}{r}\frac{\partial}{\partial r}(KT)+B \tag{8}$$

where

$$B=-\left[\frac{\partial S}{\partial t}+\frac{\partial(uS)}{\partial r}+\frac{\partial(vS)}{\partial z}\right]$$

$$C(T)=\begin{bmatrix} C_{sl} & (T<-\delta T)\\ \frac{1}{2}(1+C_{sl})+\frac{1}{2Ste\delta T} & (-\delta T\leqslant T\leqslant\delta T)\\ 1 & (T>\delta T)\end{bmatrix} \tag{9}$$

$$S(T)=\begin{bmatrix} C_{sl}\delta T & (T<-\delta T)\\ \frac{1}{2}(1+C_{sl})\delta T+\frac{1}{2Ste} & (-\delta T\leqslant T\leqslant\delta T)\\ C_{sl}\delta T+\frac{1}{Ste} & (T>\delta T)\end{bmatrix} \tag{10}$$

$$K(T)=\begin{bmatrix} K_{sl} & (T<-\delta T)\\ K_{sl}+\frac{(1-K_{sl})(T+\delta T)}{2\delta T} & (-\delta T\leqslant T\leqslant\delta T)\\ 1 & (T>\delta T)\end{bmatrix}. \tag{11}$$

2.3. *Gas dynamics*

In this model the temperature is assumed to be continuous across the melt/vapor interface which is an extension of an earlier model by Von Allmen [4]. In a nonequilibrium situation, the melt surface properties are determined from the conservation of mass, momentum and energy fluxes across the melt/vapor interface, as shown in Fig. 2. Relative to fixed reference frame, the velocity at which the melt surface moves will be denoted by $\vec{\mathbf{v}}_{\ell v}$ and the velocities of the melt and vapor will be denoted by $\vec{\mathbf{v}}_m$ and $\vec{\mathbf{v}}_v$, respectively. In the arguments to follow, a local coordinate system which rides with the melt surface element will be constructed, with $\hat{\mathbf{n}}$ defined to be the outward unit vector to the surface element. In the local moving frame the velocities of the melt and vapor leaving the melt surface will be denoted by $\vec{\mathbf{u}}_m$ and $\vec{\mathbf{u}}_v$. These velocities are related by

$$\vec{\mathbf{u}}_m=\vec{\mathbf{v}}_m-\vec{\mathbf{v}}_{\ell v}\quad \vec{\mathbf{u}}_v=\vec{\mathbf{v}}_v-\vec{\mathbf{v}}_{\ell v}. \tag{12}$$

Temperatures at the melt surface, in the vapor and in the melt will be denoted as T_s, T_v and T_m, respectively. Assuming the temperature to be continuous across the melt/vapor interface and taking T_v and T_m to be very close to the melt surface gives $T_s\equiv T_m\equiv T_v$.

In the moving reference frame, the mass, the momentum and the energy balances across the melt/vapor interface may be written [17] as,

$$\rho_m\vec{\mathbf{u}}_m\cdot\hat{\mathbf{n}}=\rho_v\vec{\mathbf{u}}_v\cdot\hat{\mathbf{n}} \tag{13}$$

$$p_m\hat{\mathbf{n}}+\rho_m\vec{\mathbf{u}}_m(\vec{\mathbf{u}}_m\cdot\hat{\mathbf{n}})=P_v\hat{\mathbf{n}}+\rho_v\vec{\mathbf{u}}_v(\vec{\mathbf{u}}_v\cdot\hat{\mathbf{n}}) \tag{14}$$

$$\vec{I}\cdot\hat{\mathbf{n}}+L_v\rho_m\vec{\mathbf{u}}_m\cdot\hat{\mathbf{n}}+k\vec{\nabla}T]_s\cdot\hat{\mathbf{n}}=0. \tag{15}$$

Equation (15) states the energy balance among the laser energy flux, evaporative flux and the conduction flux into the melt. Some studies in the literature indicate that the gas velocity leaving the surface is nearly sonic [18] at the laser intensities typical of laser drilling. Thus, the assumptions that $T_v=T_s$ near the melt/vapor interface and ideal gas behavior of the vapor lead to the approximation $\mathbf{v}_v\simeq c_s=\sqrt{\gamma RT_s}$,

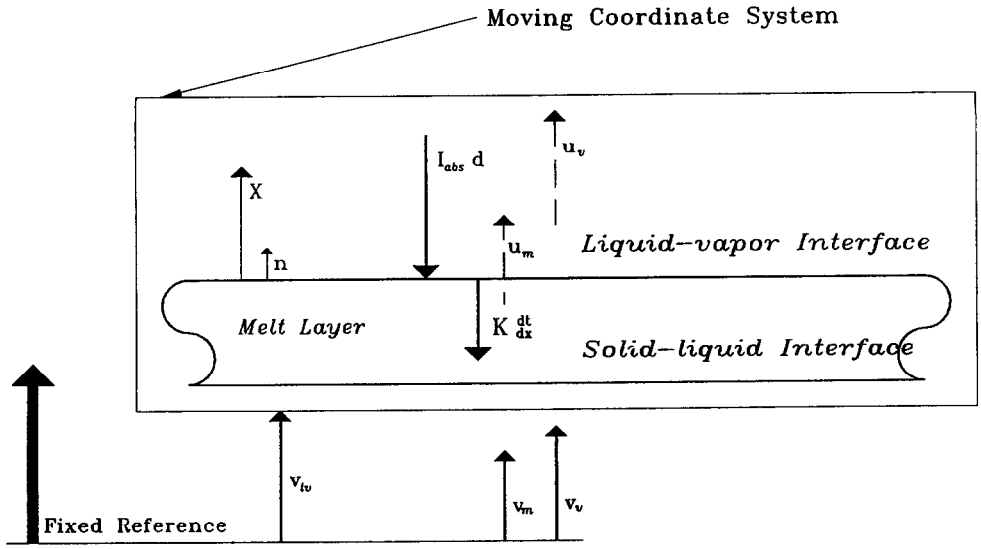

Fig. 2. Boundary conditions for gas dynamics.

where $\mathbf{v}_v = |\vec{\mathbf{v}}_v|$. Since $\mathbf{v}_v \gg |\vec{\mathbf{v}}_{tv}|$ and $\rho_m \gg \rho_v$, equations (12) and (13) imply $u_v \gg u_m$ and $u_v \simeq \mathbf{v}_v$, leading to

$$u_v \simeq \sqrt{\gamma R T_s}. \tag{16}$$

Previous calculations of the temperature gradient in the melt show that the tangential component along the melt/vapor interface is negligible compared to the normal component [19] and the approximation can be made that $\vec{\mathbf{u}}_v$ (and thus $\vec{\mathbf{u}}_m$) is normal to the melt/vapor interface. Thus equations (13)–(15) can be written in one dimension as

$$\rho_m u_m = \rho_v u_v \tag{13a}$$

$$p_m + \rho_m u_m^2 = p_v + \rho_v u_v^2 \tag{14a}$$

$$I_{abs} - L_v \rho_m u_m - k\frac{\partial T}{\partial n} = 0 \tag{15a}$$

where I_{abs} is the rate of energy absorption, $u_m \equiv |\vec{\mathbf{u}}_m|$, $u_v \equiv |\vec{\mathbf{u}}_v|$. The system of equations is completed using the ideal gas law

$$p_v = R\rho_v T_v \tag{17}$$

and the Clausius/Clapeyron equation [20]

$$p(T_s) = p_{vap,0} \exp\left[\frac{L_v}{R}\left(\frac{1}{T_{vap,0}} - \frac{1}{T_s}\right)\right]. \tag{18}$$

Identifying the surface pressure to be used in the fluid calculations as being the pressure just below the melt/vapor surface ($p_m = p_s$), using $T_s \equiv T_v$ at the melt/vapor surface and with some algebraic manipulation it can be shown

$$\frac{\gamma+1}{L_v \gamma}\sqrt{\gamma R T_s}\left(I_{abs} - k\frac{\partial T}{\partial n}\right) = p_{vap,0} \exp\left[\frac{L_v}{R}\left(\frac{1}{T_{vap,0}} - \frac{1}{T_s}\right)\right] \tag{19}$$

In practice, equation (19) is evaluated for two cases. At higher beam intensities ($I_{abs} > 0.1$ MW/cm^2) heat conduction into the melt is small compared to the rate of energy absorption and the temperature gradient term $\partial T/\partial n$ may be neglected. In this limit T_s and p_s respond instantly to changes in I_{abs}. At lower beam intensities, the flow velocity of the vapor is small and neglecting u_v in equation (15a) gives the approximation $\partial T/\partial n = I_{abs}/k$. In both cases T_s and p_s are determined as functions of the absorbed beam intensity.

2.4. *Boundary conditions*

Proper boundary conditions have to be set at all mesh boundaries, surfaces of all internal obstacles and at the free surface. The placement of the field variables and the fictitious cells outside the fluid domain are shown in Fig. 3. At the mesh boundaries, a layer of fictitious cells surrounding the mesh is used to enforce different boundary conditions. The center line of the cylinder will act like a rigid-slip wall, hence the normal velocity must be zero and the tangential velocity should have no normal gradient, i.e. (setting $i = 2$ in Fig. 2).

$$u_{1,j} = 0.0$$
$$v_{1,j} = v_{2,j} \quad \text{for } \forall j. \tag{20}$$

If the same left boundary in the Fig. 2 is assumed to be a no-slip rigid wall, then the tangential velocity component at the wall should also be zero, i.e. (setting $i = 2$ in Fig. 2),

$$u_{1,j} = 0.0$$
$$v_{1,j} = -v_{2,j} \quad \text{for } \forall j. \tag{21}$$

For the pressure and volume of fluid function F, the boundary conditions are

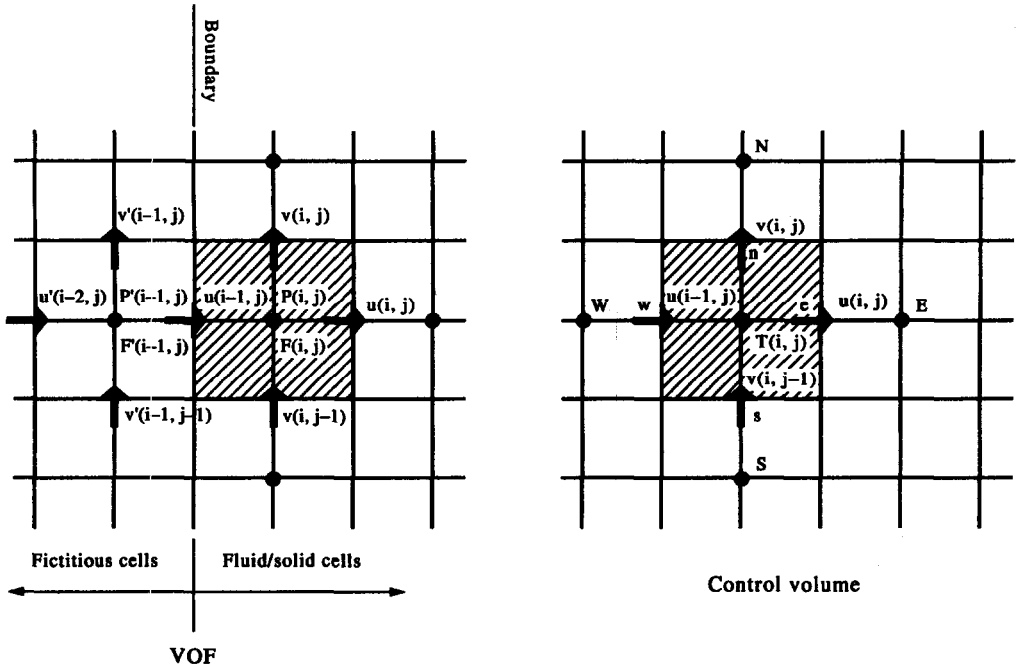

Fig. 3. Placement of field variables and fictitious cell: the location of velocity components are the same for both the VOF (no temperature variable) and the control volume method (temperature variable at the center).

$$p_{1,j} = p_{2,j}$$
$$F_{1,j} = F_{2,j} \quad \text{for } \forall j. \tag{22}$$

These conditions are imposed on the velocities to be computed from the momentum equations and also during the pressure iteration in the solution algorithm for volume of fluid method (VOF). At the free surface boundary, a normal stress boundary condition is applied which takes into account the sum of the externally impressed pressure as computed by the gas dynamics model and the one due to surface tension effect. The surface cell pressure though, is set equal to the value obtained by a linear interpolation between the impressed pressure on the surface and the pressure inside the fluid of the adjacent full fluid cell.

Zero temperature gradient (insulated) boundary conditions are imposed on the left, right and the bottom boundaries. At the left boundary, for example,

$$T_{1,j} = T_{2,j} \quad \text{for } \forall j. \tag{23}$$

These temperature boundary conditions are imposed for the solution of the advection–diffusion thermal energy equation. The free surface temperature boundary condition is set by constraining the temperature at the surface by the temperature computed by the gas dynamics model. Outside the range of the laser beam, however, the temperature is gradually decreased in an exponential manner to ambient temperature.

For a sufficiently high absorbed laser beam, the boundary conditions for the melted pool are

$$T = T_v(\vec{r}, t; I_{abs})$$

at the liquid–vapor interface (explicit)

$$T = T_m$$

at the solid–liquid interface (implicit) (24)

where T_m is the temperature of melting and T_v is the vaporization temperature which is a function of position, time and the absorbed laser intensity, i.e. the incoming laser beam intensity corrected for the orientation of the impinging surface. For the absorbed intensity range where the energy conducted into the material is more or less equal to the energy going into the latent heat of vaporization, the temperature at the melt/vapor interface is not known *a priori* and must be determined as part of the solution and therefore a natural boundary (Neumann) condition, namely, a temperature gradient boundary condition is applied which is calculated from the energy flux balance due to the incoming laser beam, heat conduction into the target and the latent heat of vaporization as given by equation (15). This type of boundary condition is called the Stefan boundary condition. In principle, a similar flux boundary condition should exist at the liquid–solid interface, but the temperature transforming model described here takes care of the boundary condition at the liquid–solid interface in an implicit manner. As far as the initial conditions are concerned, the substrate is assumed to be at ambient temperature and to start the process the top layer cells are prescribed to be free surface liquid (melt) cells.

2.5. *Assumptions*

The assumptions for the laser drilling model comprising the multi-phase heat transfer, fluid flow, vapo-

rization gas dynamics and the melting and solidification submodels are:

(1) The properties of the laser beam are invariant in the azimuthal direction and hence a 2-D axisymmetric (pseudo 3-D) analysis is appropriate. The laser beam intensity is a Gaussian function of space and time and can have multiple peaks in time.
(2) The specific heat c and the thermal conductivity k are different in the liquid and solid phases but constant. The density is the same in both the phases, however.
(3) The vapor behaves as an ideal monotomic gas (in the gas dynamics model).
(4) The reflectivity of the target material near the vaporization temperature is zero.
(5) Incident laser energy is instantly converted into heat and temperature changes occur quickly compared to changes in hole geometry.
(6) There is no plasma formation, the vapor is optically thin (transparent) and the light scattering due to melt ejection is negligible.

3. NUMERICAL METHODOLOGY

The hydrodynamical equations (1) and (2) are to be solved in the melt region for the velocity components and the pressure using the VOF (volume of fluid) method which preserves the free surface. In the same time step, the velocity field thus obtained is to be used in the energy equation (8) to obtain the temperature field which implicitly contains the phase front as well (because of equations (9)–(11)). The method used here is the control volume finite difference method [21]. The VOF method is also basically a finite difference method but for the donor-acceptor cell approximation that is required to handle the special function F and sustain the free surface and hence there exists a compatibility between the two methods in terms of the computational grid. This forms the critical link between the two, otherwise different methodologies enabling one to seek a temperature solution in a sequential fashion.

3.1. *VOF method (for the hydrodynamical equations)*

The VOF technique follows regions rather than boundaries through an Eulerian mesh of stationary cells. The boundary conditions are enforced by utilizing fictitious cells as explained in the previous section. The rules and the donor-acceptor flux approximation [16] used in this approach is shown in the Fig. 4. The value of F upstream and downstream of a flux boundary is used to establish a crude interface shape which is then used to compute the flux across the boundary. This method uses the pressure and the velocity as the primary dependent variables. A free surface cell is a cell that contains a nonzero value of F and has at least one neighboring cell that is empty. The donor cell and the central difference approximations are combined into a single expression with a parameter that controls the relative amount of each. The velocities appearing in the field equations evaluated at the new $n+1$ time interval depend on the pressure in the momentum equation occurring at the same $n+1$ time interval. The pressure iteration is carried out using the continuity equation not only until the implicit relationship for pressure and velocity is satisfied for all the fluid cells, but also in such a way that the pressures in all the free surface cells satisfy the applied surface pressure boundary condition furnished by the gas dynamics model. When the free surface boundary conditions are applied the conservation of mass is enforced for the free surface cells. The surface tension effect is incorporated in two steps. First, the pressure due to the surface tension is calculated as the product of the local curvature in each boundary cell and the surface tension coefficient. The second step is to impose this pressure on all interfaces. Near the walls, adhesion effects are accounted for by specifying the contact angle.

3.2. *Control volume method (for the energy equation)*

The energy equation (8) is discretized using the control volume finite difference approach. This equation is nonlinear due to equations (9)–(11) and therefore requires an iterative procedure for the solution. The velocity solution obtained on a fixed grid using the VOF method for each time step is used in the advection terms of the energy equation to obtain the temperature field on the same fixed grid. The location of temperature variables is at the center of the cell shown in Fig. 3 and the velocity components are located midway between the grid points on the control volume faces in a staggered fashion. It is important to observe that the location of placement of the velocity variables in the control volume method is the same as that for the VOF method, i.e. they are located on the faces of the control volumes. This compatibility is not surprising because, the marker and cell (MAC) method from which the VOF method was developed precedes the development of the control volume finite difference method. It is also important to note that the thermal conductivity at the interface will be evaluated using the harmonic mean and not the arithmetic mean. The free surface temperature boundary condition resulting from the gas dynamics model is applied on the free surface cell which is identified by the VOF function F. This boundary condition is applied along with the pressure boundary condition in the main routine (VOF algorithm) simply because temperature and pressure go together. This temperature boundary condition has to be communicated to the subroutine where the energy equation is solved. It is worth pointing out that the nonlinearity in the energy equation is entirely due to the incorporation of phase change capability as discussed earlier and not due to the presence of the advection terms. The velocity field remains constant during the iteration for temperatures within a time step.

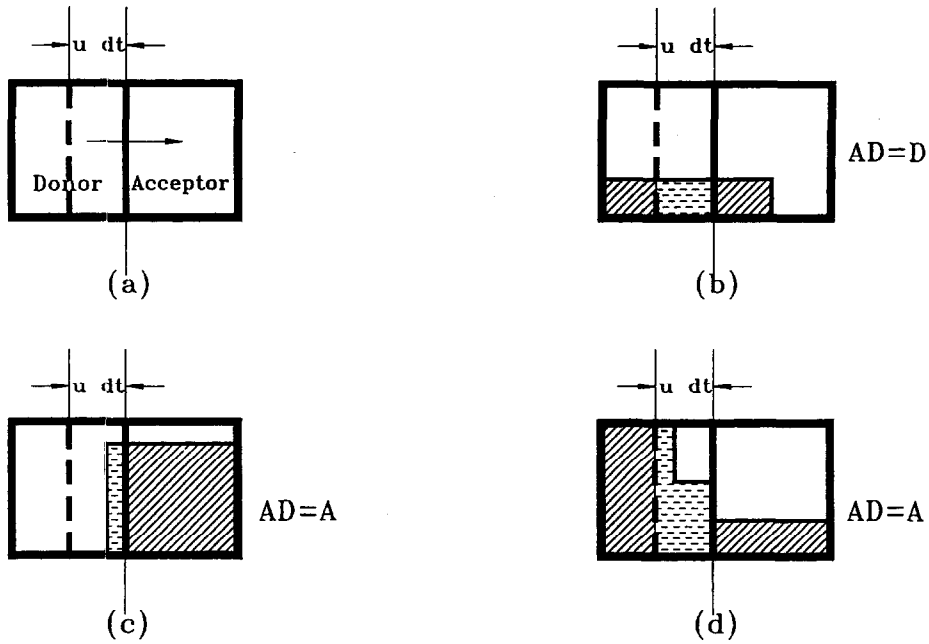

Fig. 4. Donor–acceptor flux approximation.

The velocity correction at the solid–liquid interface can be accomplished by defining the kinematic viscosity to be a function of temperature [10, 13].

$$v = \begin{bmatrix} v_l & (T > \delta T) \\ v_l + \dfrac{(v_l - N)(T - \delta T)}{2\delta T} & (-\delta T \leqslant T \leqslant \delta T) \\ N & (T < -\delta T) \end{bmatrix} \tag{25}$$

where N takes a large value. Finite difference procedures can handle large discontinuities in the diffusion coefficients and hence the method of gradually increasing the kinematic viscosity is a practical one. The value of kinematic viscosity is set equal to the fluid viscosity in the liquid region and gradually increased through the mushy region to a large value in the solid region which suppresses the velocity. It is important to note here that the no-slip velocity boundary conditions are imposed implicitly at the solid–liquid interface in the same manner the interface is tracked and hence it is easy to implement into the solution algorithm.

4. CLOSURE

This generalized thermal laser drilling model is a significantly improved version of our previous model where the melting and solidification submodel used a crude switch-on switch-off technique. A robust temperature transforming model previously tested with experiments and analytical solutions using a fixed grid numerical methodology is ideally suited for an engineering application such as this. The tracking of the solid–liquid phase front and the imposition of the no-slip velocity boundary condition at the same front is done in an implicit manner. This makes the implementation procedure less cumbersome and less tedious. It is interesting to note, however, that the velocity field obtained by the VOF method and the temperature field obtained by the control volume finite difference approach are linked together on a fixed grid.

REFERENCES

1. Bass, M., *Laser Materials Processing*. North-Holland Publishing Company, 1983.
2. Steen, W. M., *Laser Material Processing*. Springer, Berlin, 1991.
3. Luxon, J. T. and Parker, D. E., *Industrial Lasers and their Applications*, 2nd edn. Prentice Hall, 1991.
4. Von Allmen, M., Laser drilling velocity in metals. *Journal of Applied Physics*, 1976, **47**(12), 5460–5463.
5. Bellantone, R., Ganesh, R. K., Hahn, Y. and Bowley, W. W., A model of laser hole drilling: calculation with experimental comparison. *Proceedings of the 10th International Invitational Symposium on the Unification of Numerical, Analytical and Experimental Methods*, WPI, Worcester, MA 01609, 1991, pp. 317–339.
6. Ganesh, R. K., Bowley, W. W., Bellantone, R. and Hahn, Y., A model for laser hole drilling in metals. *Journal of Computational Physics*, 1996, **125**, 161–176.
7. Chan, C., Mazumder, J. and Chen, M. M., A two-dimensional transient model for convection in laser melted pool. *Metallurgical Transactions A*, 1984, **15A**, 2175–2184.
8. Basu, B. and Srinivasan, J., Numerical study of steady-state laser melting problem. *International Journal of Heat and Mass Transfer*, 1988, **31**, 2331–2338.
9. Voller, V. R., Cross, M. and Markatos, N. C., An enthalpy method for convection/diffusion phase-change. *International Journal for Numerical Methods in Engineering*, 1987, **24**, 271–284.
10. Voller, V. R. and Prakash, C., A fixed grid numerical

modelling methodology for convection–diffusion mushy region phase-change problems. *International Journal of Heat and Mass Transfer*, 1987, **30**, 1709–1719.
11. Cao, Y. and Faghri, A., A numerical analysis of phase-change problems including natural convection. *ASME Journal of Heat Transfer*, 1990, **112**(3), 812–816.
12. Cao, Y., Faghri, A. and Chang, W. S., A numerical analysis of Stefan problems for generalized multi-dimensional phase-change structures using the enthalpy transforming model. *International Journal of Heat and Mass Transfer*, 1989, **32**(7), 1289–1298.
13. Cao, Y. and Faghri, A., Thermal protection from intense localized moving heat fluxes using phase-change materials. *International Journal of Heat and Mass Transfer*, 1990, **33**(1), 127–138.
14. Zeng, X. and Faghri, A., Temperature-transforming model for binary solid–liquid phase-change problems: part I—mathematical modeling and numerical methodology. *Numerical Heat Transfer Part B—Fundamental*, 1994, **25**(4), 467–480.
15. Zeng, X. and Faghri, A., Temperature-transforming model for binary solid–liquid phase-change problems: part II—numerical simulation. *Numerical Heat Transfer Part B—Fundamental*, 1994, **25**(4), 481–500.
16. Nichols, B. D., Hirt, C. W. and Hotchkiss, R. S., *SOLA-VOF: A solution algorithm for Transient Fluid Flow with Multiple Free Boundaries*. Los Alamos Scientific Laboratory, LA-8355, 1980.
17. Landau, L. D. and Lifschitz, E. M., *Fluid Mechanics*, Pergamon Press, New York, 1959.
18. Knight, C. J., Theoretical modeling of rapid structure vaporization with back pressure. *AIAA Journal*, 1979, **17**(5), 519–523.
19. Bellantone, R., Nonequilibrium thermodynamics of laser-metal interaction. Ph.D. dissertation, Department of Physics, The University of Connecticut, 1992.
20. Callen, H., *Thermodynamics and an Introduction to Thermostatistics*. Wiley, New York, 1985.
21. Patankar, S. V., *Numerical Heat Transfer and Fluid Flow*. McGraw-Hill, New York, 1980.
22. Paek, U. C. and Gagliano, P., Thermal analysis of laser drilling process. *IEEE Journal of Quantum Electronics*, 1971, 112–119.
23. Kou, S. and Wang, Y. H., Three-dimensional convection in laser melted pools. *Metallurgical Transactions A*, 1986, **17A**, 2265–2270.
24. Mazumder, J., Overview of melt dynamics in laser processing. *Optical Engineering*, 1991, **30**(8), 1208–1219.
25. Chan, C. L. and Mazumder, J., One-dimensional steady-state model for damage by vaporization and liquid expulsion due to laser-material interaction. *Journal of Applied Physics*, 1987, **62**(11), 4579–4586.
26. Zacharia, T., Eraslan, A. H., Aidun, D. K. and David, S. A., Three-dimensional transient model for arc welding process. *Metallurgical Transactions B*, 1989, **20B**, 645–659.
27. Kar, A. and Mazumder, J., Two-dimensional model for material damage due to melting and vaporization during laser irradiation. *Journal of Applied Physics*, 1990, **68**(8), 3884–3891.
28. Patel, R. S. and Brewster, M. Q., Gas-assisted laser-metal drilling: theoretical model. *Journal of Thermophysics and Heat Transfer*, 1991, **5**(1), 32–39.
29. Kar, A. and Mazumder, J., Two-dimensional model for laser-induced material damage: effects of assist gas and multiple reflections inside the cavity. *Journal of Applied Physics*, 1992, **71**(6), 2560–2569.
30. Gordon, M. H., Touzelbaev, M., Xiao, M. and Goforth, R. C., Numerical simulation of diamond film ablation under irradiation by a laser beam. *ASME Proceedings*, Chicago, IL, 1994, pp. 73–77.
31. Ho, J. R., Grigoropolous, C. P. and Humphrey, J. A. C., Computational study of heat transfer and gas dynamics in the pulsed laser evaporation of metals. *ASME Proceedings*, Chicago, IL, 1994, pp. 71–90.